Adapting free-space fast multipole method for layered media Green's function: algorithm and analysis

Min Hyung Cho

Department of Mathematical Sciences, University of Massachusetts Lowell, Lowell, MA 01854-2874

Jingfang Huang

Department of Mathematics, University of North Carolina at Chapel Hill, Chapel Hill, NC 27599-3250

Abstract

In this paper, we present a numerical algorithm for an accurate and efficient computation of the convolution of the frequency domain layered media Green's function with a given density function. Instead of compressing the convolution matrix directly as in the classical fast multipole method, fast direct solvers, and fast $\mathcal{H}$-matrix algorithms, this new algorithm considers a translated form of the original matrix so that many existing building blocks from the highly optimized free-space fast multipole method can be easily adapted to the Sommerfeld integral representations of the layered media Green's function. An asymptotic analysis is performed on the Sommerfeld integrals for large orders to provide an estimate of the decay rate in the new "multipole" and "local" expansions. To avoid the highly oscillatory integrand in the original Sommerfeld integral representations when the source and target are close to each other, or when they are both close to the interface in the scattered field, mathematically equivalent alternative direction integral representations are introduced. The convergence of the multipole and local expansions formulas and quadrature rules for the original and alternative direction integral representations are numerically validated.

Keywords: Helmholtz Equation, Sommerfeld integral, Fast multipole method, Asymptotic analysis, Low-rank representation, Multi-layered media, Layered media Green's function
2010 MSC: 65R20, 65Z05, 78M25

*Corresponding author
Email address: huang@email.unc.edu (Jingfang Huang)

Submitted preprint

1. Introduction

Acoustic and electromagnetic wave propagation in layered media has been a very important research topic for many modern applications including solar cells [1, 2], photonic crystals [3], meta-materials [4], and applied geophysics [5]. The efficient numerical simulation of waves in layered media in the frequency domain is still a challenging task in scientific computing. One of the key numerical difficulties arises from the Sommerfeld integral representation for a general layered media Green's function [6, 7]. For example, consider a simple three-layered medium (e.g., air-sea-seabed or meta-materials) for the case of electromagnetic scattering in transverse magnetic (TM) polarization with layer interfaces at $y = 0$ and $y = -d$ and a source located in the top layer at $\mathbf{x}_0 = (x_0, y_0)$ with $y_0 > 0$ (see Figure 1). Assume k_1, k_2, and k_3 are the wave numbers and the permeability is constant in each layer. The layered-media Green's function is the solution of the Helmholtz equations

$$\Delta u_i(\mathbf{x}) + k_i^2 u_i(\mathbf{x}) = -\delta(\mathbf{x}_0, \mathbf{x}), i = 1, 2, 3$$

with interface conditions

$$u_1(\mathbf{x}) = u_2(\mathbf{x}), \frac{\partial u_1}{\partial \mathbf{n}}(\mathbf{x}) = \frac{\partial u_2}{\partial \mathbf{n}}(\mathbf{x}) \text{ for } \mathbf{x} = (x, 0),$$

$$u_2(\mathbf{x}) = u_3(\mathbf{x}), \frac{\partial u_2}{\partial \mathbf{n}}(\mathbf{x}) = \frac{\partial u_3}{\partial \mathbf{n}}(\mathbf{x}) \text{ for } \mathbf{x} = (x, -d).$$

Applying the integral transforms and matching the continuity conditions at the interfaces to reduce the differential equations to a system of algebraic equations, then inverse transforming its solutions back to the original domain, the Green's function can be analytically represented as different Sommerfeld integrals for different layers [8]. For example, the scattered field at $\mathbf{x}_1 = (x_1, y_1)$ in the middle layer ($-d < y_1 < 0$) contains the reflected field from the top and bottom interfaces. The reflected field from the top interface g_2^t (formula for the bottom interface is similar) is represented by

$$g_2^t(\mathbf{x}_1, \mathbf{x}_0) = \int_{-\infty}^{\infty} e^{\sqrt{\lambda^2 - k_2^2} y_1} e^{i\lambda x_1} e^{-\sqrt{\lambda^2 - k_1^2} y_0} e^{-i\lambda x_0} \frac{1}{4\pi\sqrt{\lambda^2 - k_2^2}} \sigma_2^t(\lambda) d\lambda$$

where

$$\sigma_2^t(\lambda) = \frac{e^{d\sqrt{\lambda^2 - k_2^2}}(\lambda^2 + \sqrt{\lambda^2 - k_2^2}\sqrt{\lambda^2 - k_3^2} - k_2^2)}{\sinh(d\sqrt{\lambda^2 - k_2^2})(\lambda^2 + \sqrt{\lambda^2 - k_1^2}\sqrt{\lambda^2 - k_3^2} - k_2^2) + \sqrt{\lambda^2 - k_2^2}(\sqrt{\lambda^2 - k_1^2} + \sqrt{\lambda^2 - k_3^2})\cosh(d\sqrt{\lambda^2 - k_2^2})}$$

is referred to as the density on the top interface [9] (see Example 3 in Section 3 for further details). A discretization of the integral equation description of the wave field in layered media leads to a linear system, where each entry in the coefficient matrix requires the evaluation of one or more of these Sommerfeld integrals [10, 11], which becomes computationally expensive, particularly when the source and target are close to the same interface, e.g., when both y_1 and y_0

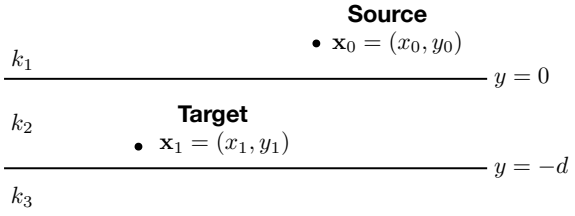

Figure 1: Three-layered medium with a source point $\mathbf{x}_0$ in the top layer and a target point $\mathbf{x}_1$ in the middle layer.

are close to the upper ($y = 0$) interface and $|x_1 - x_0| \gg |y_1 - y_0|$ in the function g_2^t. Note that even state-of-the-art fast direct solvers or $\mathcal{H}$-matrix algorithms [12, 13, 14, 15] require a sufficient number of samples of the coefficient matrix entries before the matrix can be effectively compressed for further numerical linear algebra operations.

This paper is aimed at *completely resolving* two of the many existing challenges in the simulation of waves in layered media: (a) an optimal fast algorithm for the application of the layered media Green's function to a given density function, and (b) an effective numerical scheme to compute the layered media Green's function when the source and target are close to each other, or close to the media interface. Firstly, we present a general algorithm framework for an optimal fast solver. The new algorithm compresses a transformed version of the original matrix, and both the expansions and translation operators are derived using mathematical analysis techniques. The transformed matrix approach makes it possible for the new algorithm to use many well-optimized numerical tools from existing free-space fast multipole method (FMM) with minor or no changes. This approach is different from existing FMM, fast direct solver, and fast $\mathcal{H}$-matrix algorithms which compress the coefficient matrix directly. The error analysis of the expansion is based on the asymptotic analysis of integrals which can be generalized to layered media Green's functions in three dimensions. Secondly, by introducing different integration contours for the Sommerfeld integral representation of the layered media Green's function, the new method can also effectively and accurately evaluate the interactions when either the source, or target, or both are close to the interface between different layers. The resulting algorithm complexity is asymptotically optimal $\mathcal{O}(N)$ in the low frequency regime, with a prefactor close to that of the well-developed free-space FMM algorithms.

To present these ideas, we restrict our attention to the two-dimensional (2-D) layered media in this paper and organize the paper as follows: In Section 2, we summarize all necessary building blocks for the new algorithm and present the pseudocode and complexity analysis. Section 3 provides several Green's functions examples. In Section 4, we present a detailed analysis of the numerical algorithm, including the asymptotic expansion based truncation error analysis of the new "multipole" (far-field) and "local" expansions, and the mathematically equivalent alternative direction Sommerfeld integral representations of the

original layered media Green's function. Section 5 presents numerical results designed to validate the algorithm analysis. We summarize our results and discuss future work in Section 6.

2. Adapting Free-space FMM for 2-D Layered Media Green's Functions

We first present the algorithm framework. Detailed analysis of each algorithm component will be covered in Section 4. This section is written for readers with sufficient knowledge of the classical FMM [16], which is becoming a standard topic in scientific computing.

2.1. Summary of Algorithm Building Blocks

We use notation and terminology commonly adopted by the FMM community, and present the building blocks in the same order as they appear in the algorithm.

Layered Media Green's Functions.
The layered media Green's function consists of the free-space and scattered field parts. Since the free-space Green's function is well-studied, we focus on a general form of the scattered field Green's function. For a target point $\mathbf{x} = (x, y)$ in the layer with wave number k and a source point $\mathbf{x}_0 = (x_0, y_0)$ in the layer with wave number k_0, the scattered field Green's function is given by

$$g^s(\mathbf{x}, \mathbf{x}_0) = \int_{-\infty}^{\infty} e^{-\sqrt{\lambda^2 - k^2}(y+d)} e^{i\lambda x} e^{\pm\sqrt{\lambda^2 - k_0^2} y_0} e^{-i\lambda x_0} \frac{\sigma(\lambda)}{4\pi\sqrt{\lambda^2 - k^2}} d\lambda \qquad (1)$$

where d is a constant, and the density function $\sigma(\lambda)$ is independent of $\mathbf{x}$ and $\mathbf{x}_0$ which converges to a constant when $\lambda \to \pm\infty$ (see examples in Section 3). When the "+" sign is used in $e^{\pm\sqrt{\lambda^2 - k_0^2} y_0}$, $y + d - y_0$ is assumed to be positive in order to guarantee integrability. Sample Sommerfeld integral representations of layered media Green's functions for acoustic waves and time harmonic Maxwell's equations (vector Helmholtz equations) can be found in [6, 9, 17, 18, 19] and in Section 3. Rigorous analysis of the density function properties in a general layered media setting requires a detailed study of the corresponding system of linear equations derived from the integral transforms and by matching the interface conditions. Interested readers are referred to example 3 in Section 3 for further discussions. In the following, the mathematical formulas for the "+" sign are presented. The formulas for the "−" sign can be derived in the same way and are thus omitted.

Multipole Expansion and Source-to-Multipole (S2M) Translation Operator. Assume there are N sources from the same layer located in a box centered at $\mathbf{x}_c^s = (x_c^s, y_c^s)$, each carrying a charge q_j located at $\mathbf{x}_j = (x_j, y_j)$. Their

contributions to the far-field location $\mathbf{x} = (x, y)$ are given by

$$\begin{aligned}\phi(\mathbf{x}) &= \sum_{j=1}^{N} q_j g^s(\mathbf{x}, \mathbf{x}_j) \qquad (2)\\ &= \int_{-\infty}^{\infty} e^{-\sqrt{\lambda^2-k^2}(y+d)} e^{i\lambda x} \left(\sum_{j=1}^{N} q_j e^{\sqrt{\lambda^2-k_0^2} y_j} e^{-i\lambda x_j} \right) \frac{\sigma(\lambda)}{4\pi\sqrt{\lambda^2-k^2}} d\lambda.\end{aligned}$$

Lemma 1 (Multipole Expansion). *The far-field contributions at* $\mathbf{x}$ *due to charges* q_j *located at* $\mathbf{x}_j$, $j = 1, 2, \cdots N$ *in a box centered at* $\mathbf{x}_c^s$ *in Eq. (2) have the multipole expansion*

$$\phi(\mathbf{x}) = \sum_{p=-\infty}^{\infty} M_p \Phi_p(x, y), \qquad (3)$$

where the multipole coefficient is given by

$$M_p = \sum_{j=1}^{N} q_j J_p(k_0 r_j) e^{-ip\theta_j}, \qquad (4)$$

(r_j, θ_j) *are the polar coordinates of* $\mathbf{x}_j$ *with respect to* $\mathbf{x}_c^s$, J_p *is the Bessel function of order p, the new multipole basis function is given by*

$$\Phi_p(x, y) = \int_{-\infty}^{\infty} e^{-\sqrt{\lambda^2-k^2}(y-y_c^s+d)} e^{i\lambda(x-x_c^s)} \left(\frac{\lambda - \sqrt{\lambda^2-k_0^2}}{k_0} \right)^p \frac{\tilde{\sigma}(\lambda)}{4\pi\sqrt{\lambda^2-k^2}} d\lambda, \qquad (5)$$

and $\tilde{\sigma}(\lambda) = \sigma(\lambda) e^{-\sqrt{\lambda^2-k^2} y_c^s + \sqrt{\lambda^2-k_0^2} y_c^s}$.

We refer to forming the multipole expansion in Eq. (3) as the Source-to-Multipole (S2M) operator. Eq. (4) is derived by applying the Jacobi-Anger formula [20] $e^{ikr\cos\theta} = \sum_{m=-\infty}^{\infty} i^m J_m(kr) e^{im\theta}$ to the term $\sum_{j=1}^{N} q_j e^{\sqrt{\lambda^2-k_0^2} y_j} e^{-i\lambda x_j}$. Using the new basis Φ_p instead of the classical Hankel functions, the multipole coefficients M_p in Eq. (4) become identical to those in the free-space Helmholtz FMM [21] derived using Graf's addition theorem. Therefore, the existing free-space S2M operator for the Helmholtz equation with the same wave number k_0 can be used directly to derive the coefficients M_p of the compressed representation in Eq. (3). Note that the asymptotic properties of $\tilde{\sigma}(\lambda) = \sigma(\lambda) e^{-\sqrt{\lambda^2-k^2} y_c^s + \sqrt{\lambda^2-k_0^2} y_c^s}$ remain the same as the original $\sigma(\lambda)$ as $\lambda \to \pm\infty$.

Remark: By introducing the change of variable $z = \frac{\lambda - \sqrt{\lambda^2-k_0^2}}{k_0}$ in Eq. (5), the expansion $\sum_{p=-\infty}^{\infty} M_p z^p$ is the Laurent expansion of the function

$$\sum_{j=1}^{N} q_j e^{\sqrt{\lambda^2-k_0^2}(y_j - y_c^s)} e^{-i\lambda(x_j - x_c^s)},$$

and M_p is the expansion coefficient independent of λ (or z).

At the low-frequency regime when both k_0 and k are small, the number of terms required in the truncated layered media multipole expansion for a prescribed error tolerance is approximately the same as that in the free-space Laplace FMM. We leave the truncation error analysis of the multipole (and local) expansions to Section 4.

Multipole-to-Multipole (M2M) Translation Operator. In FMM, multipole expansion of the parent is constructed by translating the multipole expansion of the children. Translating the center of a multipole expansion from a child box to its parent box is referred to as the Multipole-to-Multipole (M2M) translation operator. Since the multipole coefficients for the layered media in Eq. (4) are the same as those for the free-space Green's function for the Helmholtz equation with wave number k_0 for both the parent and child boxes, we therefore have the following lemma:

Lemma 2 (M2M). *The M2M translation operator for the layered media Green's function in Eq. (4) is the same as the M2M operator for the free-space Green's function of the Helmholtz equation with wave number k_0. The parent's multipole coefficients $\widetilde{M}_p$ are given by*

$$\widetilde{M}_p = \sum_{q=-\infty}^{\infty} M_{p-q} J_q(k_0 r_{12}) e^{iq\theta_{12}} \tag{6}$$

where M_{p-q} are the child's multipole coefficients and (r_{12}, θ_{12}) are the polar coordinates of the child's center with respect to the parent's center.

Thus, the free-space M2M translation operator can be used without any change to obtain the multipole expansions for all the boxes on the hierarchical tree structure for the *layered media Green's function*.

Local Expansion and Multipole-to-Local (M2L) Translation Operator. Notice that the potential field $\phi(\mathbf{x})$ in a particular layer satisfies the Helmholtz equation with wave number k. We therefore use the same Bessel function based expansion as that for the free-space Green's function with wave number k to compress the received far-field contributions into a local expansion of the target box centered at $\mathbf{x}_c^t = (x_c^t, y_c^t)$ entirely located within a target layer.

Lemma 3 (Local Expansion). *The potential function ϕ due to the far-field source contributions can be compressed into a local expansion*

$$\phi(\mathbf{x}) = \sum_{p=-\infty}^{\infty} L_p J_p(kr) e^{ip\theta}, \tag{7}$$

where (r, θ) are the polar coordinates of $\mathbf{x}$ with respect to the target box center $\mathbf{x}_c^t$, and L_p is called the local expansion coefficient. Evaluating the local expansion at a target point is referred to as the Local-to-Target (L2T) translation operator.

Similar to the free-space FMM, the compressed far-field multipole expansion of the source box centered at $\mathbf{x}_c^s$ given by Eq. (3) can be translated into a local expansion in Eq. (7) of the target box centered at $\mathbf{x}_c^t$, by substituting the plane wave formula

$$e^{i(\lambda(x-x_c^t)+\sqrt{k^2-\lambda^2}(y-y_c^t))} = \sum_{m=-\infty}^{\infty} i^m J_m(kr) e^{im\theta} \left(\frac{\lambda - i\sqrt{k^2-\lambda^2}}{k} \right)^m \tag{8}$$

into the basis function Φ_p from Eq. (5), where (r, θ) are the polar coordinates of $\mathbf{x}$ with respect to the target box center at $\mathbf{x}_c^t$. Translating the multipole expansion to a local expansion is referred to as the Multipole-to-Local (M2L) translation operator and we have the following lemma.

Lemma 4 (M2L). *The local expansion coefficients of a target box centered at $\mathbf{x}_c^t$, due to the contributions from particles in a source box centered at $\mathbf{x}_c^s$ described by its multipole expansion in Eq. (3), can be computed using the M2L translation matrix $\mathrm{A} = \{A_{p,q}\}$ using*

$$L_p = \sum_{q=-\infty}^{\infty} A_{p,q} M_q \tag{9}$$

where

$$\begin{aligned} A_{p,q} = \int_{-\infty}^{\infty} & i^p e^{-\sqrt{\lambda^2-k^2}(y_c^t - y_c^s + d)} e^{i\lambda(x_c^t - x_c^s)} \\ & \times \left(\frac{\lambda + \sqrt{\lambda^2-k^2}}{k} \right)^p \left(\frac{\lambda - \sqrt{\lambda^2-k_0^2}}{k_0} \right)^q \frac{\tilde{\sigma}(\lambda)}{4\pi\sqrt{\lambda^2-k^2}} d\lambda. \end{aligned} \tag{10}$$

Note that when $|y_c^t - y_c^s + d| \ll |x_c^t - x_c^s|$, the evaluation of $A_{p,q}$ can be very costly due to the highly oscillatory term $e^{i\lambda(x_c^t - x_c^s)}$. This difficulty can be resolved by using the *alternative direction* integral representation of the translation operator that will be discussed in Section 4. The translation matrix A can be precomputed for optimal efficiency when the geometries of the layered media and embedded objects are fixed, or computed on the fly using the Gauss and Laguerre quadrature rules for the *alternative direction* integral representations.

Local-to-Local (L2L) Translation Operator. The local expansion of the parent can be translated to its children using the Local-to-Local (L2L) translation operator given by the following lemma [21, 22].

Lemma 5 (L2L). *As the basis for the local expansion of the layered media Green's function is the same as that for the free-space Green's function of the Helmholtz equation with wave number k, the L2L translation operator for the layered media Green's function in Eq. (7) is therefore the same as the L2L operator of the free-space FMM for the Helmholtz equation with wave number k. The child's local coefficients $\widetilde{L}_p$ are given by*

$$\widetilde{L}_p = \sum_{q=-\infty}^{\infty} L_{p-q} J_q(kr_{12}) e^{-iq(\theta_{12}-\pi)} \tag{11}$$

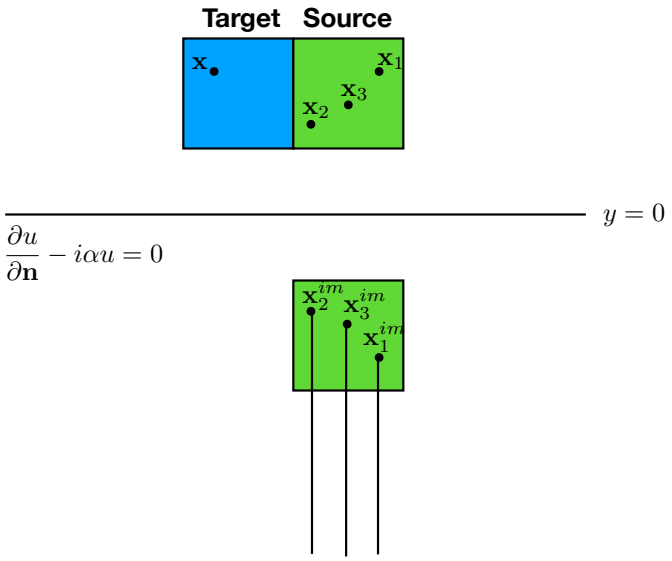

Figure 2: Source-to-Target by M2L translation. Image sources are well separated from target.

where L_{p-q} are the parent's local expansion coefficients and (r_{12}, θ_{12}) are the polar coordinates of the parent's box center with respect to the child's box center.

This lemma states that the free-space L2L translation operator can be used without change to derive the local expansion of the child box from its parent's for the layered media case.

Direct Source-to-Target (S2T) Interactions. For neighboring boxes, the interaction of the source and target can be handled in two ways: (1) by evaluating the Sommerfeld integral directly, or (2) for the scattered field contribution from sources in a source box, when its multipole expansion is also valid in its neighboring target box, e.g., due to the constant d in Eq. (5), the source box's multipole expansion can be translated and merged into the target box's local expansion using the same M2L translation operator as we discussed previously for the interaction list boxes, which will be evaluated later using the very efficient L2T operator for the leaf boxes. We demonstrate (2) using the scattered Green's function interaction of two neighboring boxes for the half-space medium with impedance boundary condition in Figure 2. When the method of images representation of the scattered Green's function is considered [19, 23], the neighbor box's contribution from particles x_1, x_2 and x_3 is equivalent to that from the far-field point- and line-images starting from x_1^{im}, x_2^{im} and x_3^{im}, and hence the neighbor's multipole expansion in Eq. (3) becomes valid. In such cases, the FMM tree can be modified accordingly to further accelerate the computation.

One numerical difficulty of evaluating the layered media Green's function for direct S2T interaction or entries of the translation matrix A in M2L comes

from the oscillatory term $e^{i\lambda x}$ when the other exponential terms in the integrand decay slowly: for example, in the free-space Green's function,

$$g(\mathbf{x}, \mathbf{x}_0) = \int_{-\infty}^{\infty} e^{-\sqrt{\lambda^2 - k^2} y} e^{i\lambda x} \frac{1}{4\pi\sqrt{\lambda^2 - k^2}} d\lambda \tag{12}$$

where the source point is located at the origin $(x_0, y_0) = (0, 0)$ and the target point is located in the first quadrant ($x > 0$ and $y > 0$). In the new version of FMM [22, 24, 25], it is referred to as the "north" plane wave expansion because this formula is valid when $y > 0$. However, when y is very close to the line $y = 0$ and $x \gg 0$, a huge number of quadrature points has to be used to resolve the oscillatory term $e^{i\lambda x}$ due to the very slow decay of $e^{-\sqrt{\lambda^2 - k^2} y}$. Similar problems arise when evaluating the direct interaction of the source and target points that are close to the interface of the layered media and the M2L translation matrix A in Eq. (9).

To understand the origin of this problem, we divide the Sommerfeld integral representation into the propagating ($|\lambda| < k$) and evanescent ($|\lambda| > k$) parts. After a change of variables as in [24], Eq. (12) can be rewritten as

$$g(\mathbf{x}, \mathbf{x}_0) = \frac{1}{4\pi} \int_0^{\pi} e^{ik(y \sin\theta - x \cos\theta)} d\theta + \frac{1}{2\pi i} \int_0^{\infty} e^{-ty} \cos(\sqrt{t^2 + k^2} x) dt.$$

The first and second integrals are called the propagating part and evanescent part, respectively. For the propagating part, the number of required Gauss quadrature points to evaluate the integral only depends on k and $r = \sqrt{x^2 + y^2}$, which is typical. However, when $y \ll x$, the integrand in the evanescent part $e^{-ty} \cos(\sqrt{t^2 + k^2} x)$ requires many Laguerre quadrature points to resolve the oscillatory term $\cos(\sqrt{t^2 + k^2} x)$ because e^{-ty} decays slowly. This problem can be resolved alternatively by using the equivalent "east" plane wave representation for $x > 0$

$$g(\mathbf{x}, \mathbf{x}_0) = \frac{1}{4\pi} \int_0^{\pi} e^{ik(-y \cos\theta + x \sin\theta)} d\theta + \frac{1}{2\pi i} \int_0^{\infty} e^{-tx} \cos(\sqrt{t^2 + k^2} y) dt,$$

which can be derived from the "north" plane wave representation using contour integration as will be discussed in Section 4. Since $y \ll x$, the evanescent part of the alternative direction integral can be evaluated using a small number of Laguerre quadrature points. Similar representations can also be derived for the "south" and "west" directions for general layered media Green's functions by using the method of images, contour integration, or applying the integral transforms directly in the alternative direction.

"Layer Conforming" Adaptive Tree Structure. In more complicated geometries, it is still an open problem how to effectively merge the multipole expansions from child boxes in two different layers, or find one unified analytical local expansion for a box containing target points from different layers. Therefore, in existing implementation, we only allow the M2L interaction of boxes that are located entirely inside a layer. This constraint requires the generation

and optimization of a "layer conforming" adaptive tree structure, which is currently being studied for general layered media settings. However, since most of practical applications have less than 10 layers, the computational complexity will increase at most by a constant factor.

2.2. Algorithm Pseudocode

We present the algorithm pseudocode in Algorithm 1. Compared with the classical FMM for free-space kernels, the adapted FMM for layered media Green's function only differs in the layer conforming adaptive tree, the M2L and S2T subroutines, and the number of expansion terms when the wave numbers are different. All other subroutines and functions from free-space FMM can be adopted with minor or no changes by the layered media FMM.

2.3. Algorithm Complexity

We compare the algorithm complexity of the layered media FMM (LM-FMM) with that of the free-space FMM (FS-FMM).

In the upward pass, only the free-space S2M and M2M translation operators are used. Thus, if the number of expansion terms is the same as that of the free-space case, the LM-FMM has the same number of operations as the FS-FMM in the upward pass. In the downward pass, the L2L operator of the LM-FMM has the same complexity as that of the FS-FMM. However, the M2L operator requires more operations when the M2L translation matrix is computed on the fly, as at least one integral has to be evaluated to find each entry of the translation matrix. Note that these integrals can be evaluated efficiently when the alternative direction integral representations are used (further discussed in Section 4). Moreover, the translation matrix can often be re-used by many boxes in the same level in the hierarchical tree structure. On the other hand, when the translation matrix A is precomputed, the algorithm complexity in the downward pass is about the same as that in the classical FS-FMM. In Step 4, the evaluation of the local expansion in the LM-FMM has the same complexity as that in the FS-FMM. For the direct source to target (S2T) interactions, more operations are needed than FS-FMM because the alternative direction Sommerfeld integrals have to be evaluated. In summary, when the local direct interaction operations are not counted (which can be very efficient on parallel computers), the translation matrix A is precomputed, and the number of expansion terms is the same as that of the FS-FMM, the total number of operations of the LM-FMM is about the same as that of the FS-FMM. In Section 4, we show that for many settings, the number of expansion terms of the LM-FMM is in the same order as that of the FS-FMM, for example, when the wave numbers of different layers are all in the low-frequency regime.

3. Examples of 2-D Layered Media Green's Functions

We consider the potential at a target point $\mathbf{x} = (x, y)$ due to a source charge with density q_0 located at $\mathbf{x}_0 = (x_0, y_0)$. The source and target may be located

Algorithm 1 Adapting Free-space FMM for Layered Media Green's Functions

Step 1: Initialization

Generate an adaptive layer conforming tree and precompute necessary tables.

Step 2: Upward Pass

for $l = L, \cdots, 0$ **do**
  for all boxes j on level l **do**
    if j is a leaf node **then**
      compute S2M using *free-space* S2M operator.
    else
      compute M2M using *free-space* M2M operator.
    end if
  end for
end for

Step 3: Downward Pass

for $l = 1, \cdots, L$ **do**
  for all boxes j on level l **do**
    shift local expansion of j's parent to j using *free-space* L2L operator.
    collect interaction list contribution using M2L operator in Eq. (9).
    collect valid neighbor box multipole expansion using M2L operator.
  end for
end for

Step 4: Evaluate Local Expansions and Direct Interactions

for each leaf node (childless box) **do**
  evaluate local expansion (L2T) at each particle location.
  collect un-evaluated source target interaction (S2T) from neighbor boxes (including self) using alternative direction Sommerfeld integrals.
end for

in the same or different layers with the j^{th} interface located at $y = y_j$. The wave numbers are k_0 for the source layer and k for the target layer, respectively.

To derive the layered media Green's function, a Fourier transform is usually performed along the x-direction, reducing the 2-D Helmholtz equation to an ODE system which can be solved analytically with some unknown density functions in the Sommerfeld integral representations. The density functions are obtained by solving a linear system of algebraic equations to match the interface conditions. In this paper, we consider the Green's function in a generalized form

$$G(\mathbf{x}, \mathbf{x}_0) = \int_{-\infty}^{\infty} e^{-\sqrt{\lambda^2-k^2}(y+d)} e^{i\lambda x} e^{\pm\sqrt{\lambda^2-k_0^2}y_0} e^{-i\lambda x_0} \frac{\sigma(\lambda)}{4\pi\sqrt{\lambda^2-k^2}} d\lambda \qquad (13)$$

where d is a constant and $\sigma(\lambda)$ converges to a constant when $\lambda \to \pm\infty$. Many 2-D layered media Green's functions are in this particular form. In the following discussions, we refer to the first two exponential terms $e^{-\sqrt{\lambda^2-k^2}(y+d)} e^{i\lambda x}$ as the target term, the third and fourth exponential terms $e^{\pm\sqrt{\lambda^2-k_0^2}y_0} e^{-i\lambda x_0}$ as the source term, and $\sigma(\lambda)$ as the image term (for reasons which will be explained later). We present a few sample Green's functions, all in the form of Eq. (13).

Example 1: Free-space Green's Function. The first example is the free-space Green's function for the Helmholtz equation with wave number k. For a source point $\mathbf{x}_0 = (x_0, y_0)$ and a target point $\mathbf{x} = (x, y)$ with $y - y_0 > 0$, the free-space Green's function is given by the Sommerfeld integral of the form

$$g(\mathbf{x}, \mathbf{x}_0) = \int_{-\infty}^{\infty} e^{-\sqrt{\lambda^2-k^2}y} e^{i\lambda x} e^{\sqrt{\lambda^2-k^2}y_0} e^{-i\lambda x_0} \frac{1}{4\pi\sqrt{\lambda^2-k^2}} d\lambda. \qquad (14)$$

Example 2: Half-space with Zero Dirichlet Boundary Condition. The second example is the half-space problem with Dirichlet condition (total field is 0) at the layer interface located at $y = 0$. We assume the source is located at $\mathbf{x}_0 = (x_0, y_0)$ in the upper half plane ($y_0 > 0$). Using the method of images, the scattered field for a target point located at $\mathbf{x} = (x, y)$ in the upper half plane ($y > 0$) can be represented as

$$g^s(\mathbf{x}, \mathbf{x}_0) = \int_{-\infty}^{\infty} e^{-\sqrt{\lambda^2-k^2}y} e^{i\lambda x} e^{-\sqrt{\lambda^2-k^2}y_0} e^{-i\lambda x_0} \frac{-1}{4\pi\sqrt{\lambda^2-k^2}} d\lambda. \qquad (15)$$

To satisfy the Dirichlet boundary condition, an image charge is added at the location $(x_0, -y_0)$ and -1 is the charge of the image source. Interested readers are referred to [26] for more details.

Example 3: Half-space with Impedance Boundary Condition. The third example is the half-space Green's function with the impedance boundary condition

$$\frac{\partial u}{\partial y} - i\alpha u = 0 \qquad (16)$$

at the layer interface $y = 0$. The scattered field at a target point $\mathbf{x} = (x, y)$ due to the source at $\mathbf{x}_0 = (x_0, y_0)$, where both points are located in the upper half

plane with wave number k, is given by

$$g^s(\mathbf{x},\mathbf{x}_0)=\int_{-\infty}^{\infty}e^{-\sqrt{\lambda^2-k^2}y}e^{i\lambda x}e^{-\sqrt{\lambda^2-k^2}y_0}e^{-i\lambda x_0}\frac{1}{4\pi\sqrt{\lambda^2-k^2}}\frac{\sqrt{\lambda^2-k^2}+i\alpha}{\sqrt{\lambda^2-k^2}-i\alpha}d\lambda. \tag{17}$$

In [19, 23], it was shown that the term $\frac{\sqrt{\lambda^2-k^2}+i\alpha}{\sqrt{\lambda^2-k^2}-i\alpha}$ can be derived using the method of complex images. We therefore refer to the $\sigma(\lambda)=\frac{\sqrt{\lambda^2-k^2}+i\alpha}{\sqrt{\lambda^2-k^2}-i\alpha}$ term as the image term. This Green's function was also discussed in [26]. Note that when $\lambda\to\pm\infty$, $\sigma\to 1$.

Example 3: Three-layered Medium with Transmission Condition. The last example we consider in this paper is the Green's function for a three-layered medium with the transmission condition in [9], where the layer interfaces are located at $y=0$ and $y=-d$ (See Figure 1). Let a source point be located in the top layer at $\mathbf{x}_0=(x_0,y_0)$ and a target point be located at $\mathbf{x}=(x,y)$. In the first layer ($y>0$), the scattered field g_1^s is the field reflected from bottom layers. In the second layer ($-d<y<0$), the scattered field consists of the contribution from top and bottom interfaces $g_2^s=g_2^t+g_2^b$. In the third layer ($y<-d$), the scattered field g_3^s is the transmitted field from the source in the first layer. By matching the continuity of the field, the scattered field in each layer can be represented as

$$\begin{aligned}
g_1^s(\mathbf{x},\mathbf{x}_0)&=\int_{-\infty}^{\infty}e^{-\sqrt{\lambda^2-k_1^2}y}e^{i\lambda x}e^{-\sqrt{\lambda^2-k_1^2}y_0}e^{-i\lambda x_0}\frac{1}{4\pi\sqrt{\lambda^2-k_1^2}}\sigma_1(\lambda)d\lambda,\\
g_2^t(\mathbf{x},\mathbf{x}_0)&=\int_{-\infty}^{\infty}e^{\sqrt{\lambda^2-k_2^2}y}e^{i\lambda x}e^{-\sqrt{\lambda^2-k_1^2}y_0}e^{-i\lambda x_0}\frac{1}{4\pi\sqrt{\lambda^2-k_2^2}}\sigma_2^t(\lambda)d\lambda,\\
g_2^b(\mathbf{x},\mathbf{x}_0)&=\int_{-\infty}^{\infty}e^{-\sqrt{\lambda^2-k_2^2}(y+2d)}e^{i\lambda x}e^{-\sqrt{\lambda^2-k_1^2}y_0}e^{-i\lambda x_0}\frac{1}{4\pi\sqrt{\lambda^2-k_2^2}}\sigma_2^b(\lambda)d\lambda,\\
g_3^s(\mathbf{x},\mathbf{x}_0)&=\int_{-\infty}^{\infty}e^{-\sqrt{\lambda^2-k_3^2}(y+2d)}e^{i\lambda x}e^{-\sqrt{\lambda^2-k_1^2}y_0}e^{-i\lambda x_0}\frac{1}{4\pi\sqrt{\lambda^2-k_3^2}}\sigma_3(\lambda)d\lambda
\end{aligned}$$

where $(\sigma_1(\lambda),\sigma_2^t(\lambda),\sigma_2^b(\lambda),\sigma_3(\lambda))^T$ is the solution of the linear system

$$\begin{pmatrix}
-1 & \frac{\sqrt{\lambda^2-k_1^2}}{\sqrt{\lambda^2-k_2^2}} & \frac{e^{-d\sqrt{\lambda^2-k_2^2}}\sqrt{\lambda^2-k_1^2}}{\sqrt{\lambda^2-k_2^2}} & 0\\
0 & e^{-d\sqrt{\lambda^2-k_2^2}} & 1 & -\frac{\sqrt{\lambda^2-k_2^2}}{\sqrt{\lambda^2-k_3^2}}\\
1 & 1 & -e^{-d\sqrt{\lambda^2-k_2^2}} & 0\\
0 & e^{-d\sqrt{\lambda^2-k_2^2}} & -1 & -1
\end{pmatrix}
\begin{pmatrix}\sigma_1(\lambda)\\ \sigma_2^t(\lambda)\\ \sigma_2^b(\lambda)\\ \sigma_3(\lambda)\end{pmatrix}=
\begin{pmatrix}1\\0\\1\\0\end{pmatrix}. \tag{18}$$

The solution $(\sigma_1(\lambda), \sigma_2^t(\lambda), \sigma_2^b(\lambda), \sigma_3(\lambda))^T$ is explicitly given by

$$\begin{pmatrix} \frac{\sinh\left(d\sqrt{\lambda^2-k_2^2}\right)\left(-\lambda^2+\sqrt{\lambda^2-k_1^2}\sqrt{\lambda^2-k_3^2}+k_2^2\right)+\sqrt{\lambda^2-k_2^2}\left(\sqrt{\lambda^2-k_1^2}-\sqrt{\lambda^2-k_3^2}\right)\cosh\left(d\sqrt{\lambda^2-k_2^2}\right)}{\sinh\left(d\sqrt{\lambda^2-k_2^2}\right)\left(\lambda^2+\sqrt{\lambda^2-k_1^2}\sqrt{\lambda^2-k_3^2}-k_2^2\right)+\sqrt{\lambda^2-k_2^2}\left(\sqrt{\lambda^2-k_1^2}+\sqrt{\lambda^2-k_3^2}\right)\cosh\left(d\sqrt{\lambda^2-k_2^2}\right)} \\ \frac{e^{d\sqrt{\lambda^2-k_2^2}}\left(\lambda^2+\sqrt{\lambda^2-k_2^2}\sqrt{\lambda^2-k_3^2}-k_2^2\right)}{\sinh\left(d\sqrt{\lambda^2-k_2^2}\right)\left(\lambda^2+\sqrt{\lambda^2-k_1^2}\sqrt{\lambda^2-k_3^2}-k_2^2\right)+\sqrt{\lambda^2-k_2^2}\left(\sqrt{\lambda^2-k_1^2}+\sqrt{\lambda^2-k_3^2}\right)\cosh\left(d\sqrt{\lambda^2-k_2^2}\right)} \\ -\frac{e^{d\sqrt{\lambda^2-k_2^2}}\left(-\lambda^2+\sqrt{\lambda^2-k_2^2}\sqrt{\lambda^2-k_3^2}+k_2^2\right)}{\sinh\left(d\sqrt{\lambda^2-k_2^2}\right)\left(\lambda^2+\sqrt{\lambda^2-k_1^2}\sqrt{\lambda^2-k_3^2}-k_2^2\right)+\sqrt{\lambda^2-k_2^2}\left(\sqrt{\lambda^2-k_1^2}+\sqrt{\lambda^2-k_3^2}\right)\cosh\left(d\sqrt{\lambda^2-k_2^2}\right)} \\ \frac{2\sqrt{\lambda^2-k_2^2}\sqrt{\lambda^2-k_3^2}e^{d\sqrt{\lambda^2-k_3^2}}}{\sinh\left(d\sqrt{\lambda^2-k_2^2}\right)\left(\lambda^2+\sqrt{\lambda^2-k_1^2}\sqrt{\lambda^2-k_3^2}-k_2^2\right)+\sqrt{\lambda^2-k_2^2}\left(\sqrt{\lambda^2-k_1^2}+\sqrt{\lambda^2-k_3^2}\right)\cosh\left(d\sqrt{\lambda^2-k_2^2}\right)} \end{pmatrix}.$$

Note that when $\lambda \to \pm\infty$, each σ function converges to a constant.

The form of the Green's function in Eq. (13) is not surprising. Clearly, the first target term satisfies the Helmholtz equation at the target layer with wave number k, and the source term satisfies the Helmholtz equation at the source layer with wave number k_0. The third term is independent of the variables $\mathbf{x}_0$ and $\mathbf{x}$, and we collect all the exponential growth or decay terms in the constant d in the target term so the image term converges to a constant when $\lambda \to \pm\infty$.

4. Analysis of Layered Media Fast Multipole Method

We present a detailed analysis of the algorithm for layered media Green's function in this section. We focus on the following two topics: (a) the number of terms in the multipole and local expansions and truncation errors, and (b) evaluation of the local direct interactions and M2L translation operators using the mathematically equivalent alternative direction Sommerfeld integral representation.

4.1. Truncating the Multipole and Local Expansions

We study the decay rates of the terms in the multipole and local expansions by considering the setting of a single source with a unit charge located at $\mathbf{x}_0 = (x_0, y_0)$. The multipole expansion describes the potential at far-field locations as a function of $\mathbf{x} = (x, y)$ due to a charge in the source box, namely,

$$\phi(\mathbf{x}) = \sum_{p=-\infty}^{\infty} M_p \Phi_p(x, y), \quad M_p = J_p(k_0 r) e^{-ip\theta},$$

where (r, θ) are the polar coordinates of the point (x_0, y_0) with respect to the source box center $\mathbf{x}_c^s = (x_c^s, y_c^s)$. The basis function $\Phi_p(\mathbf{x})$ is given by

$$\Phi_p(\mathbf{x}) = \int_{-\infty}^{\infty} e^{-\sqrt{\lambda^2-k^2}(y-y_c^s+d)} e^{i\lambda(x-x_c^s)} \left(\frac{\lambda-\sqrt{\lambda^2-k_0^2}}{k_0}\right)^p \frac{\tilde{\sigma}(\lambda)}{4\pi\sqrt{\lambda^2-k^2}} d\lambda \tag{19}$$

and we define the "modified" distance between $\mathbf{x}$ and $\mathbf{x}_c^s$ of the multipole expansion as $\rho = \sqrt{(y-y_c^s+d)^2+(x-x_c^s)^2}$. The multipole expansion can be

considered as a compressed representation of the source box's contribution to be sent to the far-field locations. Similarly, the local expansion associated with each target box compresses the received far-field contributions and describes the potential as a function of $(x - x_c^t, y - y_c^t)$ given by

$$\phi(\mathbf{x}) = \sum_{p=-\infty}^{\infty} L_p J_p(k\tilde{r}) e^{ip\tilde{\theta}} = \sum_{p=-\infty}^{\infty} J_p(k\tilde{r}) e^{ip\tilde{\theta}} \Psi_p(x_0, y_0),$$

where $(\tilde{r}, \tilde{\theta})$ are the polar coordinates of the point (x, y) with respect to the target box center $\mathbf{x}_c^t = (x_c^t, y_c^t)$. The basis function $\Psi_p(\mathbf{x}_0)$ is given by

$$\Psi_p(\mathbf{x}_0) = \int_{-\infty}^{\infty} \left(\frac{\lambda - i\sqrt{k^2 - \lambda^2}}{k} \right)^p e^{-\sqrt{\lambda^2 - k_0^2}(y_c^t + d - y_0)} e^{i\lambda(x_c^t - x_0)} \frac{\tilde{\tilde{\sigma}}(\lambda)}{4\pi\sqrt{\lambda^2 - k^2}} d\lambda \tag{20}$$

where $\tilde{\tilde{\sigma}}(\lambda) = \sigma(\lambda) e^{-\sqrt{\lambda^2 - k^2} y_c^t + \sqrt{\lambda^2 - k_0^2} y_c^t}$. We define the "modified" distance between $\mathbf{x}_0$ and $\mathbf{x}_c^t$ of the local expansion as $\tilde{\rho} = \sqrt{(y_c^t - y_0 + d)^2 + (x_c^t - x_0)^2}$.

Similar to the FS-FMM where the truncation errors of the multipole and local expansions are determined by the decay rate of $|J_p(kr)H_p(k\rho)|$, we study the decay rate of the term $|J_p(k_0 r)\Phi_p(x, y)|$ for the multipole expansion, and $|J_p(kr)\Psi_p(x_0, y_0)|$ for the local expansion for different physical parameter settings. When all other variables are fixed, $J_p \to 0$ and $H_p, \Phi_p, \Psi_p \to \infty$ as $p \to \infty$. Therefore, it is necessary to understand the asymptotic behavior of these functions for large p values.

Asymptotic Forms of Bessel Functions for Large Order. The asymptotic expansion for large-order Bessel functions is a well-studied topic. We cite the following well-known results from [20], which are valid for fixed z when $\nu \to \infty$.

$$J_\nu(z) \sim \frac{1}{\sqrt{2\pi\nu}} \left(\frac{ez}{2\nu} \right)^\nu, \tag{21}$$

$$Y_\nu(z) \sim -iH_\nu^{(1)}(z) \sim iH_\nu^{(2)}(z) \sim -\sqrt{\frac{2}{\pi\nu}} \left(\frac{ez}{2\nu} \right)^{-\nu}. \tag{22}$$

Therefore, for the free-space Green's function,

$$|J_{p+1}(k_0 r)H_{p+1}(k_0\rho)| / |J_p(k_0 r)H_p(k_0\rho)| \sim \frac{r}{\rho},$$

and the truncation errors of both the free-space multipole and local expansions decay exponentially as $p \to \infty$ [21].

Asymptotic Approximation of Integrals. The asymptotic expansion for the Bessel functions can be derived from the integral representations of these special functions. Note that these integral representations are similar to the layered media Green's functions. Therefore the same asymptotic analysis techniques can be applied, and the results can be used to derive more precise error

bounds when truncating the layered media multipole and local expansions. We demonstrate this ideas using the following examples.

We start with the integral representation of the Bessel function [20],

$$\begin{aligned} J_n(z) &= \frac{i^{-n}}{2\pi}\int_{-\pi}^{\pi} e^{iz\cos\theta}\cos(n\theta)d\theta \\ &= \frac{i^{-n}}{2\pi}\int_{-\pi}^{\pi}\sum_{k=0}^{\infty}\frac{(iz\cos\theta)^k}{k!}\cos(n\theta)d\theta \\ &= i\sum_{k=0}^{\infty}\frac{i^{-n}}{2\pi}\frac{(iz)^k}{k!}\int_{-\pi}^{\pi}(\cos\theta)^k\cos(n\theta)d\theta. \end{aligned}$$

Note that when $k < n$, the integral $\int_{-\pi}^{\pi}(\cos\theta)^k\cos(n\theta)d\theta = 0$. By applying Stirling's formula $n! \sim \sqrt{2\pi n}(\frac{n}{e})^n$ to the leading order of the expansion, one recovers the asymptotic form of the Bessel function for large orders in Eq. (21). This asymptotic expansion is valid for all z values and provides a more accurate estimate when studying the truncation error in the multipole and local expansions, especially in the low frequency regime when $k_0 r$ and kr are small.

For the layered media Green's function, both integrals in the basis functions Φ_p and Ψ_p can be formulated as

$$\int_{-\infty}^{\infty} e^{-\sqrt{\lambda^2-k_1^2}y}e^{i\lambda x}\left(\frac{\lambda-\sqrt{\lambda^2-k_2^2}}{k_2}\right)^p\frac{\sigma(\lambda)}{4\pi\sqrt{\lambda^2-k_1^2}}d\lambda \tag{23}$$

where k_1 is the wave number in the target layer and k_2 is the wave number in the source layer. The integral can be divided into three parts, when (a) $|\lambda| < \min\{k_1, k_2\}$, (b) $|\lambda| > \max\{k_1, k_2\}$, and (c) $\min\{k_1, k_2\} \le |\lambda| \le \max\{k_1, k_2\}$. The asymptotic expansion for each part can be derived using existing asymptotic analysis techniques for integrals [27]. When $k_1 = k_2$, the integral in (a) is often referred to as the "propagating" part and the integral in (c) becomes the "evanescent" part. The asymptotic properties of the basis functions Φ_p and Ψ_p are determined by the "propagating" part for large $||\mathbf{x}||$ values with fixed p, and by the "evanescent" part for large p values with fixed $||\mathbf{x}||$. To understand the truncation errors in the multipole and local expansions of the layered media Green's function, we therefore focus on the evanescent part and demonstrate the asymptotic analysis for the simplified integral

$$\int_0^{\infty} e^{-ty}e^{i\sqrt{t^2+k_1^2}x}\left(\frac{\sqrt{t^2+k_1^2}+\sqrt{t^2+k_1^2-k_2^2}}{k_2}\right)^p\frac{\tilde{\sigma}(t)}{4\pi\sqrt{t^2+k_1^2}}dt, \tag{24}$$

where we assume $k_1 > k_2$. The case when $k_1 < k_2$ can be analyzed in a similar way. Instead of deriving the asymptotic expansion of Eq. (24) directly, we adopt the following steps to further simplify the integral to a more standard form that is commonly used when analyzing the asymptotic behavior of the Bessel functions. First, using the polar coordinates (r, θ) of (x, y), we rewrite

the $\{x, y\}$-related exponential part as

$$e^{-ty}e^{i\sqrt{t^2+k_1^2}x} = e^{-k_1 r\left(\frac{t\sin(\theta)}{k_1} - \frac{i\cos(\theta)\sqrt{k_1^2+t^2}}{k_1}\right)}.$$

Second, we define a new variable $u = \frac{t\sin(\theta)}{k_1} - \frac{i\cos(\theta)\sqrt{k_1^2+t^2}}{k_1}$. Clearly, the new integral for the u-variable is on a complex contour, not on the real axis. Third, using contour integration and the residue theorem, we can rewrite the integral on the complex contour back to the sum of an integral on the real axis and an easy-to-analyze integral on a line segment in the complex plane (which will be explained in detail in Section 4.2). Finally, we focus on the asymptotic expansion of the dominating integral

$$\int_0^\infty e^{-k_1 ru}\left(\frac{\beta(u)+\sqrt{\beta^2(u)-k_2^2}}{k_2}\right)^p \frac{\tilde{\tilde{\sigma}}(u)}{4\pi\sqrt{1+u^2}}du = \int_0^\infty e^{-k_1 ru}\left(f(u)\right)^p g(u)du,$$

where $\beta(u) = k_1\left(\sqrt{u^2+1}\sin(\theta) - iu\cos(\theta)\right)$ and $\tilde{\tilde{\sigma}}(u) = \tilde{\sigma}(t(u))$. For any fixed $z = k_1 r$, one approach to find the asymptotic behavior of this integral is to first perform another change of variable $\lambda = k_1 ru = zu$ (or $u = \frac{\lambda}{k_1 r} = \frac{\lambda}{z}$) and consider the new integral

$$\int_0^\infty e^{-\lambda}\left(f(\frac{\lambda}{z})\right)^p g(\frac{\lambda}{z})\frac{d\lambda}{z} = (k_2 r)^{-p}\int_0^\infty e^{-\lambda}\left(\tilde{\beta}(z)+\sqrt{\tilde{\beta}^2(z)-(\frac{k_2}{k_1}z)^2}\right)^p \tilde{g}(\frac{\lambda}{z})d\lambda$$

where $\tilde{\beta}(z) = \sqrt{\lambda^2+z^2}\sin(\theta) - i\lambda\cos(\theta)$. Under proper conditions, the function $\left(\tilde{\beta}(z)+\sqrt{\tilde{\beta}^2(z)-(\frac{k_2}{k_1}z)^2}\right)^p \tilde{g}(\frac{\lambda}{z})$ is an analytic function for z values on the right-half complex plane away from the origin. Thus, we can consider its Taylor expansion

$$\left(\tilde{\beta}(z)+\sqrt{\tilde{\beta}^2(z)-(\frac{k_2}{k_1}z)^2}\right)^p \tilde{g}(\frac{\lambda}{z}) = \sum_{k=0}^\infty t_k(\lambda, p, \frac{k_2}{k_1})z^k$$

as a function of z. Then, the integral representation of the evanescent part can be derived as

$$(k_2 r)^{-p}\sum_{k=0}^\infty\left(\int_0^\infty e^{-\lambda}t_k(\lambda, p, \frac{k_2}{k_1})d\lambda\right)z^k.$$

The leading order term of the expansion for very large p values is approximately

$$(k_2 r)^{-p}e^{ip\theta_0}\int_0^\infty e^{-\lambda}(2\lambda)^p d\lambda$$

for some constant θ_0, which has the same asymptotic properties as the Hankel function $H_p(k_2 r)e^{ip\theta_0}$. Note that the expansion can be used to study the properties of both the case when $p \to \pm\infty$, or when z is small (low-frequency regime). Without presenting the details, we summarize our results in the following theorem.

Theorem 1. (1) *The multipole and local expansions satisfy the following convergence estimates for large p values,*

$$|J_{p+1}(k_1 r)\Phi_{p+1}(x,y)|/|J_p(k_1 r)\Phi_p(x,y)| \sim \frac{r}{\rho}, \tag{25}$$

$$|J_{p+1}(k_2 r)\Psi_{p+1}(x_0,y_0)|/|J_p(k_2 r)\Psi_p(x_0,y_0)| \sim \frac{r}{\tilde{\rho}} \tag{26}$$

where r is the distance from the particle to its box center and ρ (or $\tilde{\rho}$) is the "modified" distance between the box center and far-field point. Both d and $\pm$ sign are considered to correct the ρ (or $\tilde{\rho}$) value. For example, $\rho = \sqrt{(y - y_c^s + d)^2 + (x - x_c^s)^2}$ for $\Phi(x,y)$ in Eq. (5) and $\tilde{\rho} = \sqrt{(y_c^t + d - y_0)^2 + (x_c^t - x_0)^2}$ for $\Psi(x_0,y_0)$ in Eq. (20).
(2) *When the wave numbers k_1 and k_2 are small, the required number of terms in the multipole and local expansions for a prescribed accuracy in the layered media FMM is approximately the same as that in the free-space FMM.*

This theorem simply states that both the multipole and local expansions in the layered media FMM are exponentially convergent and presents the asymptotic convergence rates.
Remark: When the frequency is zero, the asymptotic analysis results are the same as that from the standard FMM error analysis for the Laplace equation. In particular, $p = 9$, 18, 27, and 36 for 3-, 6-, 9-, and 12-digit accuracy, respectively. When the frequency increases, more terms are required. Estimates of the asymptotic regime and implicit relations between p and layered media settings are further studied in Section 5 (see Figures 6 and 7).
Remark: Note that when using the "modified" distance, the truncated multipole expansion of the scattered field Green's function may become valid for a neighboring (including self) target box, and therefore can be translated to its neighbor's local expansion using the M2L operator instead of the more expensive S2T operator. See Figure 2 for the method of images interpretation.

Laplace Transform and Complex Images. For many layered media Green's functions, one can justify that the inverse Laplace transform of $\tilde{\tilde{\sigma}}(z)$ can be derived using the Fourier-Mellin integral formula

$$\mathcal{L}^{-1}\{\tilde{\tilde{\sigma}}\}(t) = \frac{1}{2\pi i}\lim_{T\to\infty}\int_{\gamma-iT}^{\gamma+iT} e^{zt}\tilde{\tilde{\sigma}}(z)dz$$

where the integration is done along the vertical line $\mathrm{Re}(z) = \gamma$ in the complex plane and γ is greater than the real part of all singularities of $\tilde{\tilde{\sigma}}(z)$, so that the image part in the layered media Green's function can be represented as

$$\tilde{\tilde{\sigma}}(\lambda) = \int_0^\infty e^{-\sqrt{\lambda^2 - k_0^2}(t-\gamma_0)} f(t)dt$$

for some γ_0 which may be the same as γ. Substituting this representation into

the original layered media Green's function in Eq. (13), we have

$$G(\mathbf{x},\mathbf{x}_0)=\int_0^{\infty}\int_{-\infty}^{\infty}\frac{e^{-\sqrt{\lambda^2-k^2}(y+d)}e^{i\lambda x}}{4\pi\sqrt{\lambda^2-k^2}}e^{\pm\sqrt{\lambda^2-k_0^2}y_0-\sqrt{\lambda^2-k_0^2}(t-\gamma_0)}e^{-i\lambda x_0}f(t)d\lambda dt. \tag{27}$$

In this new representation, $f(t)$ can be considered as the complex image located at $(x_0,\pm y_0-t)$. For many layered media, it is sufficient to analyze the convergence of the multipole and local expansions of the layered media Green's functions for *each* t-mode where the new source box center is at $(x_c^s,\pm y_c^s-(t-\gamma_0))$. In [23], this complex image approach is applied to the 2-D half-space layered medium Green's function with impedance boundary conditions (see Example 3 of Section 3), and it becomes straightforward to verify using the complex images that for the same prescribed accuracy requirement, the number of expansion terms for the layered medium case is no more than that for the free-space case. Another application of the complex image approach is for the direct source-target (S2T) interactions. For a neighboring source box, when all the complex images of the scattered field are well-separated from the target box, the source box's multipole expansion becomes applicable, and it is more efficient to translate the multipole expansion to a local expansion of the target box (see Figure 2). This technique is used in [23] to compute the scattered field part of the source-target interactions.

Precomputed Tables for Number of Expansion Terms. In practice, both the asymptotic expansion and complex image approach only give a very rough estimate of the number of terms required in different expansions of the layered media Green's function. A more practical approach is to precompute a table (or table of tables) for different layered media settings. This approach is problem dependent. We are constructing such tables for several real world applications, and results will be reported in the future.

4.2. Alternative Direction Sommerfeld Integral Representations

Another difficulty in simulating waves in layered media is when the source and target are very close to each other, or when the source and target are close to the interface of different layers for the scattered field. In these cases, the computation of layered media Green's function and the M2L translation operator becomes extremely expensive. For example, when $y-y_0>0$ is close to zero and $|x-x_0|$ is relatively a big number in the Sommerfeld integral representation of the free-space Green's function in Eq. (14) or the half-space layered medium Green's function with impedance boundary conditions in Eq. (17), the exponential term $e^{-\sqrt{\lambda^2-k^2}(y-y_0)}$ decays slowly and the highly oscillatory term $e^{i\lambda(x-x_0)}$ must be sufficiently sampled. A similar problem occurs for the M2L operator in Eq. (9). When the ratio of $(y_c^t-y_c^s+d)/|x_c^t-x_c^s|$ is small, a wide range of λ values must be sampled before the integrand decays to zero sufficiently.

The numerical difficulty is not from any inherent properties of the original physical problem, rather, it is the result of using an inefficient integral representation in the numerical computation. For the same Hankel function $H_0(\beta r)$,

which is the Green's function of the free-space Helmholtz equation, a common practice is to divide $\mathbf{R}^2$ into four *overlapping regions*–North, South, East, West–corresponding to points $(x, y) \in \mathbf{R}^2$ with $y > 0, y < 0, x > 0, x < 0$, respectively. In each region, the plane wave representation of $H_0(\beta r)$ takes the following forms:

$$H_0(\beta r) = \tag{28}$$
$$\begin{cases} \frac{1}{\pi}\int_0^{\pi} e^{i\beta(y\sin\theta - x\cos\theta)}d\theta + \frac{1}{i\pi}\int_0^{\infty} \frac{e^{-ty}}{\rho_\beta(t)}\left(e^{i\rho_\beta(t)x} + e^{-i\rho_\beta(t)x}\right)dt & \textbf{North}, \\ \frac{1}{\pi}\int_0^{\pi} e^{i\beta(-y\sin\theta - x\cos\theta)}d\theta + \frac{1}{i\pi}\int_0^{\infty} \frac{e^{ty}}{\rho_\beta(t)}\left(e^{i\rho_\beta(t)x} + e^{-i\rho_\beta(t)x}\right)dt & \textbf{South}, \\ \frac{1}{\pi}\int_0^{\pi} e^{i\beta(-y\cos\theta + x\sin\theta)}d\theta + \frac{1}{i\pi}\int_0^{\infty} \frac{e^{-tx}}{\rho_\beta(t)}\left(e^{i\rho_\beta(t)y} + e^{-i\rho_\beta(t)y}\right)dt & \textbf{East}, \\ \frac{1}{\pi}\int_0^{\pi} e^{i\beta(-y\cos\theta - x\sin\theta)}d\theta + \frac{1}{i\pi}\int_0^{\infty} \frac{e^{tx}}{\rho_\beta(t)}\left(e^{i\rho_\beta(t)y} + e^{-i\rho_\beta(t)y}\right)dt & \textbf{West}, \end{cases}$$

where $\rho_\beta(t) = \sqrt{t^2 + \beta^2}$, and (r, θ) are the polar coordinates of the point (x, y). For higher order Hankel functions $H_l(\beta r)e^{il\theta}$, we have the following integral representations:

$$H_l(\beta r)e^{il\theta} =$$
$$\begin{cases} \frac{i^l}{\pi}\int_0^{\pi} e^{i\beta(y\sin\theta - x\cos\theta)}e^{-il\theta}d\theta + \\ \frac{(-i)^l}{i\pi}\int_0^{\infty} \frac{e^{-ty}}{\rho_\beta(t)}\left(e^{i\rho_\beta(t)x}\left(\frac{\rho_\beta(t)-t}{\beta}\right)^l + e^{-i\rho_\beta(t)x}\left(\frac{-\rho_\beta(t)-t}{\beta}\right)^l\right)dt & \textbf{North}, \\ \frac{i^l}{\pi}\int_0^{\pi} e^{i\beta(-y\sin\theta - x\cos\theta)}e^{il\theta}d\theta + \\ \frac{(-i)^l}{i\pi}\int_0^{\infty} \frac{e^{ty}}{\rho_\beta(t)}\left(e^{i\rho_\beta(t)x}\left(\frac{\rho_\beta(t)+t}{\beta}\right)^l + e^{-i\rho_\beta(t)x}\left(\frac{-\rho_\beta(t)+t}{\beta}\right)^l\right)dt & \textbf{South}, \\ \frac{1}{\pi}\int_0^{\pi} e^{i\beta(x\sin\theta - y\cos\theta)}e^{il\theta}d\theta + \\ \frac{(-1)^l}{i\pi}\int_0^{\infty} \frac{e^{-tx}}{\rho_\beta(t)}\left(e^{i\rho_\beta(t)y}\left(\frac{-\rho_\beta(t)-t}{\beta}\right)^l + e^{-i\rho_\beta(t)y}\left(\frac{\rho_\beta(t)-t}{\beta}\right)^l\right)dt & \textbf{East}, \\ \frac{(-1)^l}{\pi}\int_0^{\pi} e^{i\beta(-x\sin\theta - y\cos\theta)}e^{-il\theta}d\theta + \\ \frac{(-1)^l}{i\pi}\int_0^{\infty} \frac{e^{tx}}{\rho_\beta(t)}\left(e^{i\rho_\beta(t)y}\left(\frac{-\rho_\beta(t)+t}{\beta}\right)^l + e^{-i\rho_\beta(t)y}\left(\frac{\rho_\beta(t)+t}{\beta}\right)^l\right)dt & \textbf{West}, \end{cases}$$

where the first and the second integrals in each formula are called the propagating part and evanescent part, respectively. These directional representations have been applied in the *new version* of FMM in both two and three dimensions [22, 25, 28, 29]. They are also effective tools to compute the lattice sums of the free-space Green's functions [30, 31]. In these formulation, the oscillation of the integrand in the propagating part is controlled by βr, and hence no numerical quadrature issues arise. For the evanescent part at overlapping regions, e.g., when both $x, y > 0$, both the North and East integral representations are valid and can be applied. However their numerical properties are very different. Clearly, when $y/x \gg 1$, the North formula is preferred, and when $y/x \ll 1$, the East formula can be computed more efficiently using existing quadrature techniques.

The alternative direction integral can be derived using contour integration and the residue theorem in two dimensions. Similar techniques are applied

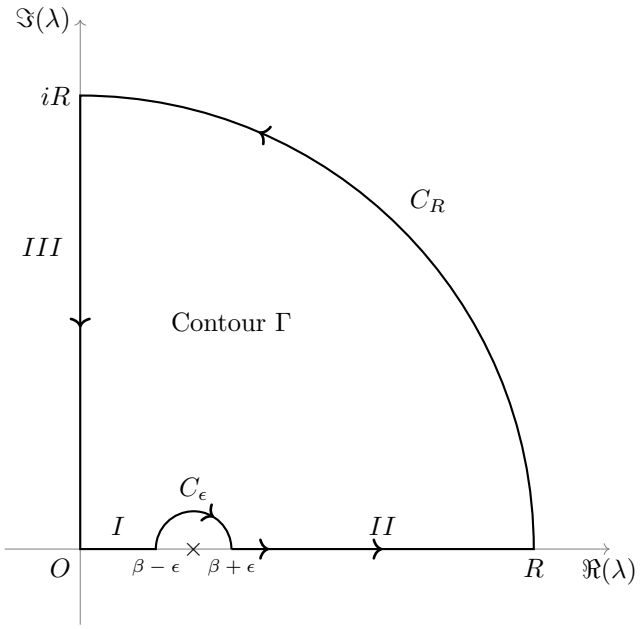

Figure 3: Contour Integral

when evaluating integrals with highly oscillatory integrands and when deriving the Schelkunoff formulation for the Sommerfeld integrals in the engineering community [32, 33]. To demonstrate how this technique works, we consider the contour integral for $x, y > 0$ in Figure 3

$$\frac{1}{\pi}\int_\Gamma \frac{e^{i(\lambda x+\sqrt{\beta^2-\lambda^2}y)}}{\sqrt{\beta^2-\lambda^2}}d\lambda. \tag{29}$$

Since there are no singularities or branch cut points inside the contour Γ, we have

$$\frac{1}{\pi}\int_\Gamma \frac{e^{i(\lambda x+\sqrt{\beta^2-\lambda^2}y)}}{\sqrt{\beta^2-\lambda^2}}d\lambda = \int_I + \int_{C_\epsilon} + \int_{II} + \int_{C_R} + \int_{III} = 0. \tag{30}$$

As $\epsilon \to 0$ and $R \to \infty$,

$$\frac{1}{\pi}\int_{C_\epsilon} \frac{e^{i(\lambda x+\sqrt{\beta^2-\lambda^2}y)}}{\sqrt{\beta^2-\lambda^2}}d\lambda \to 0 \quad , \quad \frac{1}{\pi}\int_{C_R} \frac{e^{i(\lambda x+\sqrt{\beta^2-\lambda^2}y)}}{\sqrt{\beta^2-\lambda^2}}d\lambda \to 0,$$

and

$$\frac{1}{\pi}\int_I \frac{e^{i(\lambda x+\sqrt{\beta^2-\lambda^2}y)}}{\sqrt{\beta^2-\lambda^2}}d\lambda \to \frac{1}{\pi}\int_0^\beta \frac{e^{i(\lambda x-\sqrt{\beta^2-\lambda^2}y)}}{-\sqrt{\beta^2-\lambda^2}}d\lambda,$$
$$\frac{1}{\pi}\int_{II} \frac{e^{i(\lambda x+\sqrt{\beta^2-\lambda^2}y)}}{\sqrt{\beta^2-\lambda^2}}d\lambda \to \frac{1}{\pi}\int_\beta^\infty \frac{e^{i(\lambda x+i\sqrt{\lambda^2-\beta^2}y)}}{i\sqrt{\lambda^2-\beta^2}}d\lambda,$$
$$\frac{1}{\pi}\int_{III} \frac{e^{i(\lambda x+\sqrt{\beta^2-\lambda^2}y)}}{\sqrt{\beta^2-\lambda^2}}d\lambda \to \frac{1}{\pi}\int_0^\infty \frac{ie^{(-tx-i\sqrt{t^2+\beta^2}y)}}{\sqrt{t^2+\beta^2}}dt.$$

Therefore, the evanescent part in $\int_{II}$ can be computed using $-\left(\int_I+\int_{III}\right)$. In fact, the East plane wave representation can be re-derived from the North one using this approach for $x, y > 0$.

For each Sommerfeld integral representation describing the interaction of particles either in the same layer or two different layers, a few alternative direction representations are derived analytically by choosing proper integration contours depending on the layered media geometry and wave number settings. We present more details in Section 5. In the algorithm implementation, depending on the location of the evaluation point (e.g., the ratio of $(x-c)/(y-d)$ and sign of $x-c$), one of these (mathematically equivalent but numerically different) formulas is selected and efficiently evaluated using standard quadrature rules.

5. Preliminary Numerical Experiments

In this section, we present numerical experiments to validate our theoretical analysis of the general numerical framework. Matlab and Mathematica codes are developed to numerically validate the analysis presented in Section 4.

Alternative Direction Sommerfeld Integral Representation. We have studied and validated the alternative direction Sommerfeld integral formulas for several layered media Green's functions using Mathematica. Different direction plane wave representations of the free-space Green's function presented in Section 4.2 can be readily found from existing literature [30, 31]. Therefore, we focus on the results for the half-space layered medium with impedance boundary condition. The three layered medium Green's functions can be handled in a very similar way. Interested readers are referred to the Mathematica files for these formulas, as well as their validations.

For the half-space layered medium Green's function, we focus on the evanescent part of the Green's function given by

$$\int_0^\infty \frac{e^{-ty}e^{ix\sqrt{t^2+k^2}}}{\sqrt{t^2+k^2}}\frac{(t+i\alpha)}{(t-i\alpha)}dt. \tag{31}$$

To avoid the pole on the imaginary axis, we have numerically tested the following two contours. In the first contour (left of Figure 4), a positive c value is chosen

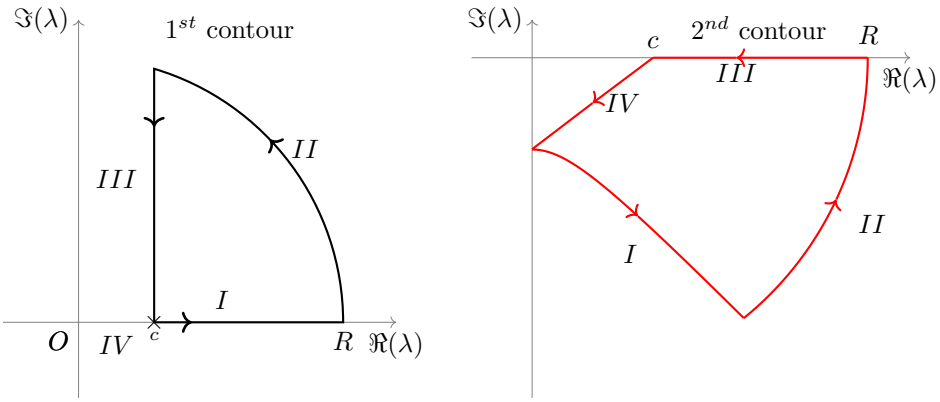

Figure 4: Two different contours for half-space layered medium with impedance boundary condition.

so that

$$\int_0^\infty \frac{e^{-ty}e^{ix\sqrt{t^2+k^2}}}{\sqrt{t^2+k^2}}\frac{(t+i\alpha)}{(t-i\alpha)}dt = \left(\int_0^c + \int_c^\infty\right)\frac{e^{-ty}e^{ix\sqrt{t^2+k^2}}}{\sqrt{t^2+k^2}}\frac{(t+i\alpha)}{(t-i\alpha)}dt.$$

As the first term integrates from 0 to c on a finite (and reasonably small by proper choice of c) line segment (labeled IV), it can therefore be efficiently evaluated using standard Gauss quadrature rules. For the second integral, as the sum of the contour integrals on $I + II + III$ is 0 and the integral on II approaches 0 when $R \to \infty$, the alternative direction representation of the integral

$$\int_c^\infty \frac{e^{-ty}e^{ix\sqrt{t^2+k^2}}}{\sqrt{t^2+k^2}}\frac{(t+i\alpha)}{(t-i\alpha)}dt$$

is given by

$$ie^{-cy}\int_0^\infty \frac{e^{-\lambda x}e^{-i\lambda y}}{\sqrt{(c+i\lambda)^2+k^2}}e^{ix\left(\sqrt{(c+i\lambda)^2+k^2}-\sqrt{(i\lambda)^2}\right)}\frac{((c+i\lambda)+i\alpha)}{((c+i\lambda)-i\alpha)}d\lambda. \quad (32)$$

This representation is numerically validated using Mathematica's `NIntegrate` with options `AccuracyGoal`→`20`, `PrecisionGoal`→`20`, `WorkingPrecision`→`60`, `MaxRecursion`→`100`, `Method`→`DoubleExponential` for different $x, y > 0$ values.

In the second contour (right of Figure 4), we assume (r, θ) are the polar coordinates of (x, y), and perform the change of variable $u = \frac{t}{k}\sin\theta - i\frac{\sqrt{t^2+k^2}}{k}\cos\theta$. The evanescent part then becomes

$$\int_I \frac{e^{-kru}}{\sqrt{1+u^2}}\frac{ik\cos\theta\sqrt{1+u^2}+uk\sin\theta+i\alpha}{ik\cos\theta\sqrt{1+u^2}+uk\sin\theta-i\alpha}du,$$

where the contour I is a curve defined by $z(t) = \frac{t}{k}\sin\theta - i\frac{\sqrt{t^2+k^2}}{k}$ for $t \in [0, \infty)$. As the integral on II approaches 0 when $R \to \infty$, the evanescent part becomes

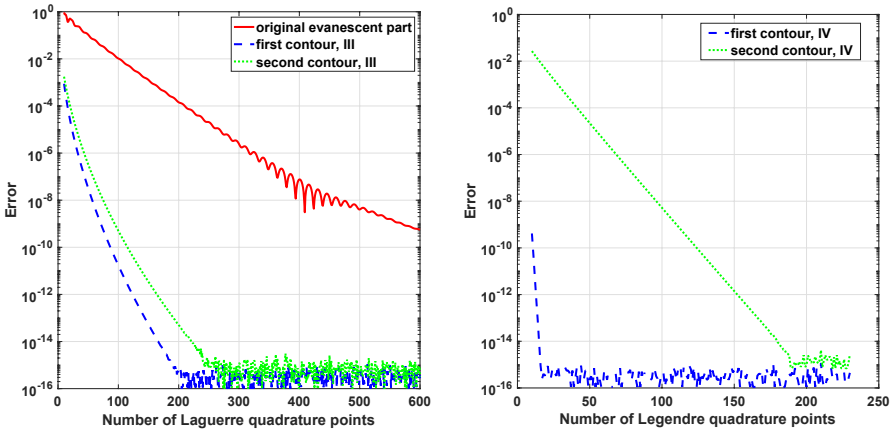

Figure 5: Convergence of the quadrature rules for different integrals.

the (negative) sum of the integrals on III and IV, given by

$$\int_c^\infty \frac{e^{-kru}}{\sqrt{1+u^2}} \frac{\phi(u)+i\alpha}{\phi(u)-i\alpha} du \tag{33}$$

and

$$\int_0^1 \frac{e^{-kr\psi(u)}}{\sqrt{1+\psi(u)^2}} \frac{\phi(\psi(u))+i\alpha}{\phi(\psi(u))-i\alpha} (c+i\cos\theta) du, \tag{34}$$

where $\phi(u) = ik\cos\theta\sqrt{1+u^2} + uk\sin\theta$, $\psi(u) = (c+i\cos\theta)u - i\cos\theta$, and c is a constant to be optimized so that both the Gauss quadrature applied on IV and Laguerre quadrature on III converge rapidly. These formulas are also validated using Mathematica for different (x, y) and c values. Note that in the second contour, the oscillatory term $e^{i\lambda x}$ or $e^{i\lambda y}$ is completely removed from the integrand, at the cost of a new rational function on a contour closer to the singularities.

We have numerically tested the convergence of the quadrature rules for the original and mathematically equivalent alternative direction representations of the half-space layered medium Green's function. In Figure 5, we set $x = 1$, $y = 0.1$, $k = 1$, and $c = 2$, and present the numerical errors when different numbers of nodes are used in the quadrature rules for different integrals. The reference solutions are computed using Mathematica requesting more than 20 correct digits. On the left of Figure 5, we present the accuracy when different numbers of Laguerre quadrature nodes are used for the original evanescent part in Eq. (31), the integral on III of the first contour in Eq. (32), and the integral on III of the second contours in Eq. (33). When $y \ll x$, the original integral converges slowly due to the oscillatory term $e^{i\sqrt{t^2+k^2}x}$. The Laguerre quadrature for the alternative direction integrals, on the other hand, converges much faster.

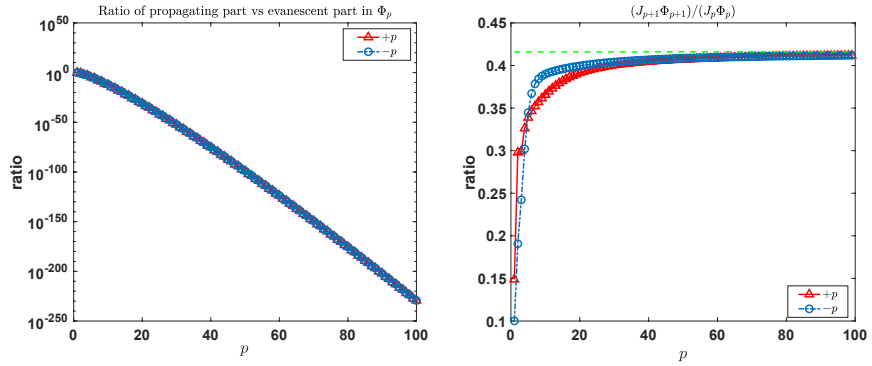

Figure 6: Convergence of the multipole expansions for impedance half-space layered medium.

For a fair comparison, we also present the convergence of the quadrature rules for the integrals on finite line segments. When Legendre polynomial-based Gauss quadrature is applied to the integral IV on both the first and second contours, for double precision requirement, under the current setting of c, approximately 17 nodes are required for the integral IV on the first contour, while around 200 Gauss nodes are required for the integral IV on the second contour. In our numerical implementation, since the formulas for the first contour are easy to derive and manipulate, we therefore adopt the first contour for the evanescent part of a general layered media Green's function.

Convergence of Multipole and Local Expansions. As we have discussed in Section 4.1, the convergence of the multipole and local expansions is determined by the ratio of r/ρ, where r is the distance between the source (target) and center of the source (target) box in the multipole (local) expansion, and ρ is the "modified" distance between the far-field target (source) and center of the source (target) box (constant d and $\pm$ sign are considered). We have numerically validated the analysis. In Figure 6, we present the results for the half-space layered medium with impedance boundary conditions using settings $x_{target} - x_c^s = 2$, $y_{target} + y_c^s = 3$, $r = 1.5$, $k = 0.1$, $\alpha = 1$, and the modified distance $\rho = \sqrt{(x_{target} - x_c^s)^2 + (y_{target} + y_c^s)^2}$. On the left of the Figure, we compare the propagating and evanescent parts of the basis Φ_p for different p values. Clearly, for large order p, the propagating part can be neglected when analyzing the truncation errors. On the right, we plot the ratio $(J_{p+1}\Phi_{p+1})/(J_p\Phi_p)$ as $p \to \pm\infty$. As $|p|$ increases, the ratio approaches the constant r/ρ (dashed green line).

A similar analysis is performed for the three-layered medium Green's function with wave numbers k_1, k_2, and k_3 in each layer. In the numerical experiment, we set $k_1 = 1$, $k_2 = 3$, $k_3 = 1$ and consider the contribution from the upper layer ($y = 0$)

$$g_2^t(\mathbf{x}, \mathbf{x}_0) = \int_{-\infty}^{\infty} e^{\sqrt{\lambda^2 - k_2^2}y} e^{i\lambda x} e^{-\sqrt{\lambda^2 - k_1^2}y_0} e^{-i\lambda x_0} \frac{1}{4\pi\sqrt{\lambda^2 - k_2^2}} \sigma_2^t(\lambda) d\lambda,$$

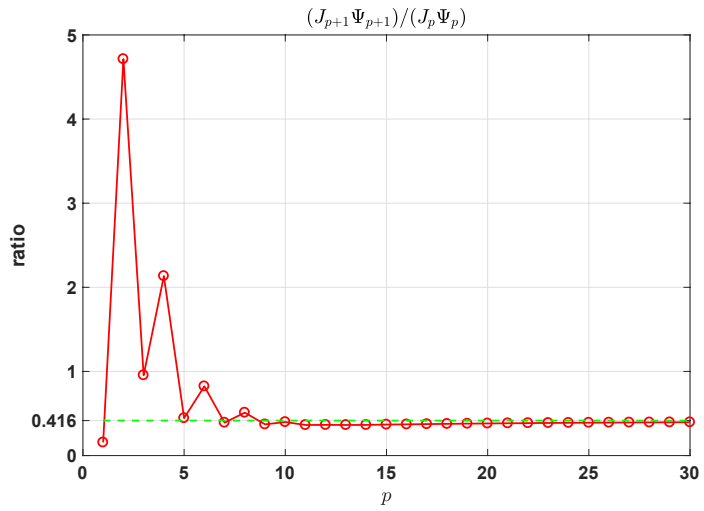

Figure 7: Convergence of the local expansion for the three-layered medium Green's function.

where

$$\sigma_2^t(\lambda) = \frac{e^{d\sqrt{\lambda^2-k_2^2}}(\lambda^2+\sqrt{\lambda^2-k_2^2}\sqrt{\lambda^2-k_3^2}-k_2^2)}{\sinh(d\sqrt{\lambda^2-k_2^2})(\lambda^2+\sqrt{\lambda^2-k_1^2}\sqrt{\lambda^2-k_3^2}-k_2^2)+\sqrt{\lambda^2-k_2^2}(\sqrt{\lambda^2-k_1^2}+\sqrt{\lambda^2-k_3^2})\cosh(d\sqrt{\lambda^2-k_2^2})}.$$

We study the convergence of the local expansion where the basis function $\Psi_p(x_0, y_0)$ is given by

$$\Psi_p(x_0,y_0) = \int_{-\infty}^{\infty}\left(\frac{\lambda - i\sqrt{k_2^2-\lambda^2}}{k_2}\right)^p e^{-\sqrt{\lambda^2-k_2^2}(y_0-y_c^t)}e^{i\lambda(x_0-x_c^t)} \times e^{(-\sqrt{k_2^2-\lambda^2}+\sqrt{k_1^2-\lambda^2})y_0}\frac{\sigma_2^t(\lambda)}{4\pi\sqrt{\lambda^2-k_2^2}}d\lambda. \tag{35}$$

We set $x_0 - x_c^t = 2$, $y_0 - y_c^t = 3$. Therefore, the modified distance $\rho = \sqrt{2^2+3^3}$. The distance between the target and center of the target box is $r = 1.5$. We neglect the propagating part in the layered medium Green's function that is very small compared with the evanescent part for large orders, and only consider the integral from k_2 to ∞ in the evanescent part of the basis function Ψ_p. In Figure 7, we show the ratio $(J_{p+1}\Psi_{p+1})/(J_p\Psi_p)$, which clearly converges to $r/\rho \approx 0.416$ as $p \to \infty$.

6. Conclusion and Generalization

In this paper, we present a general numerical framework for the efficient application of the layered media Green's function to a given density function. Instead of constructing and compressing the matrix directly, which involves the

expensive evaluations of one or more Sommerfeld-type integrals for each matrix entry, the new algorithm considers a transformed matrix, so existing fast algorithms for the free-space Green's function can be readily adapted for better algorithm efficiency. Theoretical analysis on the convergence of the new expansions and alternative direction Sommerfeld integral representations to accelerate the convergence of the numerical quadrature rules are provided and numerically validated. Similar to deriving the layered media Green's functions, the detailed translations, alternative direction Sommerfeld integral representations, and number of terms in the expansions all depend on the geometric settings and physical parameters, especially in three dimensions. We have studied a few examples of such layered media Green's functions in this paper, and we are working on both the analysis and implementation details for other important settings from domain applications. In particular, we are studying the *optimal* alternative direction Sommerfeld integral representations and more accurate estimations of the number of expansion terms necessary in different scenarios. Results from these investigations will be presented in the future.

Acknowledgement

J. Huang was supported by the NSF grant DMS1821093, and the work was finished while he was visiting professors at the King Abdullah University of Science and Technology, National Center for Theoretical Sciences (NCTS) in Taiwan, Mathematical Center for Interdisciplinary Research of Soochow University, and Institute for Mathematical Sciences of the National University of Singapore. M.H. Cho was supported by a grant from the Simons Foundation (No. 404499).

References

[1] H. A. Atwater, A. Polman, Plasmonics for improved photovoltaic devices, Nature Materials 9 (3) (2010) 205–213.

[2] M. D. Kelzenberg, S. W. Boettcher, J. A. Petykiewicz, D. B. Turner-Evans, M. C. Putnam, E. L. Warren, J. M. Spurgeon, R. M. Briggs, N. S. Lewis, H. A. Atwater, Enhanced absorption and carrier collection in Si wire arrays for photovoltaic applications, Nature Materials 9 (3) (2010) 239–244.

[3] J. D. Joannopoulos, S. G. Johnson, J. N. Winn, R. D. Meade, Photonic crystals: molding the flow of light, Princeton University Press, 2011.

[4] C. M. Soukoulis, M. Wegener, Past achievements and future challenges in the development of three-dimensional photonic metamaterials, Nature Photonics 5 (9) (2011) 523.

[5] B. Ursin, Review of elastic and electromagnetic wave propagation in horizontally layered media, Geophysics 48 (8) (1983) 1063–1081.

[6] W. C. Chew, Waves and fields in inhomogeneous media, Vol. 522, IEEE press New York, 1995.

[7] W. Cai, Algorithmic issues for electromagnetic scattering in layered media: Green's functions, current basis, and fast solver, Advances in Computational Mathematics 16 (2-3) (2002) 157–174.

[8] M. H. Cho, W. Cai, A parallel fast algorithm for computing the Helmholtz integral operator in 3-d layered media, Journal of Computational Physics 231 (2012) 5910—-5925.

[9] J. Lai, M. Kobayashi, L. Greengard, A fast solver for multi-particle scattering in a layered medium, Optics Express 22 (17) (2014) 20481–20499.

[10] D. Chen, W. Cai, B. Zinser, M. H. Cho, Accurate and efficient Nyström volume integral equation method for the Maxwell equations for multiple 3-d scatterers, Journal of Computational Physics 321 (2016) 303–320.

[11] D. Chen, M. H. Cho, W. Cai, Accurate and efficient Nyström volume integral equation method for electromagnetic scattering of 3-D metamaterials in layered media, SIAM Journal on Scientific Computing 40 (1) (2018) B259–B282.

[12] L. Greengard, D. Gueyffier, P.-G. Martinsson, V. Rokhlin, Fast direct solvers for integral equations in complex three-dimensional domains, Acta Numerica 18 (2009) 243–275.

[13] W. Hackbusch, A sparse matrix arithmetic based on $\mathcal{H}$-matrices. Part I: Introduction to $\mathcal{H}$-matrices, Computing 62 (2) (1999) 89–108.

[14] W. Hackbusch, B. N. Khoromskij, A sparse $\mathcal{H}$-matrix arithmetic, Computing 64 (1) (2000) 21–47.

[15] K. L. Ho, L. Greengard, A fast direct solver for structured linear systems by recursive skeletonization, SIAM Journal on Scientific Computing 34 (5) (2012) A2507–A2532.

[16] L. Greengard, V. Rokhlin, A fast algorithm for particle simulations, Journal of computational physics 73 (2) (1987) 325–348.

[17] M. H. Cho, W. Cai, Efficient and accurate computation of electric field dyadic Green's function in layered media, Journal of Scientific Computing 71 (3) (2017) 1319–1350.

[18] T. J. Cui, W. C. Chew, Fast evaluation of Sommerfeld integrals for EM scattering and radiation by three-dimensional buried objects, IEEE Transactions on Geoscience and Remote Sensing 37 (2) (1999) 887–900.

[19] M. O'Neil, L. Greengard, A. Pataki, On the efficient representation of the half-space impedance Green's function for the Helmholtz equation, Wave Motion 51 (1) (2014) 1–13.

[20] M. Abramowitz, I. A. Stegun, Handbook of Mathematical Functions with Formulas, Graphs, and Mathematical Tables, 10th Edition, Dover, 1964.

[21] V. Rokhlin, Rapid solution of integral equations of scattering theory in two dimensions, Journal of Computational Physics 86 (2) (1990) 414–439.

[22] W. Crutchfield, Z. Gimbutas, L. Greengard, J. Huang, V. Rokhlin, N. Yarvin, J. Zhao, Remarks on the implementation of wideband FMM for the Helmholtz equation in two dimensions, Contemporary Mathematics 408 (2006) 99–110.

[23] M. H. Cho, J. Huang, D. Chen, W. Cai, A heterogeneous FMM for layered media Helmholtz equation I: Two layers in R^2, Journal of Computational Physics 369 (2018) 237–251.

[24] L. Greengard, J. Huang, V. Rokhlin, S. Wandzura, Accelerating fast multipole methods for the Helmholtz equation at low frequencies, IEEE Computational Science and Engineering 5 (3) (1998) 32–38.

[25] L. Greengard, V. Rokhlin, A new version of the fast multipole method for the Laplace equation in three dimensions, Acta Numerica 6 (1997) 229–269.

[26] J. Lai, L. Greengard, M. O'Neil, A new hybrid integral representation for frequency domain scattering in layered media, Applied and Computational Harmonic Analysis 45 (2) (2018) 359–378.

[27] R. Wong, Asymptotic approximations of integrals, Vol. 34, SIAM, 2001.

[28] H. Cheng, W. Y. Crutchfield, Z. Gimbutas, L. F. Greengard, J. F. Ethridge, J. Huang, V. Rokhlin, N. Yarvin, J. Zhao, A wideband fast multipole method for the Helmholtz equation in three dimensions, Journal of Computational Physics 216 (1) (2006) 300–325.

[29] L. F. Greengard, J. Huang, A new version of the fast multipole method for screened Coulomb interactions in three dimensions, Journal of Computational Physics 180 (2) (2002) 642–658.

[30] A. Dienstfrey, F. Hang, J. Huang, Lattice sums and the two-dimensional, periodic Green's function for the Helmholtz equation, in: Proceedings of the Royal Society of London A: Mathematical, Physical and Engineering Sciences, Vol. 457, The Royal Society, 2001, pp. 67–85.

[31] J. Huang, Integral representations of harmonic lattice sums, Journal of Mathematical Physics 40 (10) (1999) 5240–5246.

[32] W. M. Dyab, T. K. Sarkar, M. Salazar-Palma, A physics-based Green's function for analysis of vertical electric dipole radiation over an imperfect ground plane, IEEE Transactions on Antennas and Propagation 61 (8) (2013) 4148–4157.

[33] T. K. Sarkar, W. M. Dyab, M. N. Abdallah, M. Salazar-Palma, M. Prasad, S.-W. Ting, Application of the Schelkunoff formulation to the Sommerfeld problem of a vertical electric dipole radiating over an imperfect ground, IEEE Transactions on Antennas and Propagation 62 (8) (2014) 4162–4170.